Available online at www.sciencedirect.com
SCIENCE DIRECT®
Journal of Computational Physics 196 (2004) 233–258
JOURNAL OF COMPUTATIONAL PHYSICS
www.elsevier.com/locate/jcp

Vortex blob methods applied to interfacial motion

Gregory R. Baker [a], J. Thomas Beale [b,*]

[a] Department of Mathematics, Ohio State University, Columbus, OH 43210-1174, USA
[b] Department of Mathematics, Duke University, Box 90320, 224A Physics Bldg., Durham, NC 27708-0320, USA

Received 31 July 2003; accepted 28 October 2003

Abstract

We develop a boundary integral method for computing the motion of an interface separating two incompressible, inviscid fluids. The velocity integral is regularized, so that the vortex sheet on the interface is replaced by a sum of "blobs" of vorticity. The regularization allows control of physical instabilities. We design a class of high order blob methods and analyze the errors. Numerical tests suggest that the blob size should be scaled with the local spacing of the interfacial markers. For a vortex sheet in one fluid, with a first-order kernel, we obtain a spiral roll-up similar to Krasny [J. Comput. Phys. 65 (1986) 292], but the higher order kernels lead to more detailed structure. We verify the accuracy of the new method by computing a liquid–gas interface with Rayleigh–Taylor instability. We then apply the method to the more difficult case of Rayleigh–Taylor flow separating two fluids of positive density, a case for which the regularization appears to be essential, as found by Kerr and Tryggvason [both J. Comput. Phys. 76 (1988) 48; 75 (1988) 253]. We use a "blob" regularization in certain local terms in the evolution equations as well as in the velocity integral. We find strong evidence that improved spatial resolution with fixed blob size leads to a converged, regularized solution without numerical instabilities. However, it is not clear that there is a weak limit as the regularization is decreased.

AMS: 65D30; 65R20; 76B47; 76B70

Keywords: Fluid interfaces; Boundary integral method; Vortex blob; Vortex sheet; Rayleigh–Taylor instability

1. Introduction

We develop a method for computing the motion of interfaces in incompressible, inviscid flow in cases where some regularization is needed. The interface is tracked by markers which follow the fluid, using a boundary integral method; the interface can be interpreted as a vortex sheet and the markers as elements or "blobs" of vorticity. The use of "blobs" rather than points amounts to a regularization of the singular integral (2.1) for the velocity. This regularization allows control of physical instabilities in the fluid motion and permits calculation past the time of singularity formation in the exact solution. The regularized solution so

* Corresponding author.
E-mail addresses: baker@math.ohio-state.edu (G.R. Baker), beale@math.duke.edu (J.T. Beale).

0021-9991/$ - see front matter © 2003 Elsevier Inc. All rights reserved.
doi:10.1016/j.jcp.2003.10.023

obtained can be expected, at least in some cases, to approximate a weak solution of the actual motion when the regularization parameter is small. For the case of a vortex sheet with the same fluid density on each side, Krasny [26] has made a detailed study of the spiral roll-up with one regularization and found striking evidence for convergence to a weak solution. In the present work we analyze the errors in regularizing and discretizing the velocity integral (2.1) and design a class of approximations with high order accuracy. The new method, combined with earlier work [5,6], can be used to compute interfacial motion with differing densities in the two separated fluid regions. We test the theoretical conclusions numerically and apply the new method to calculations of vortex sheets with equal densities and to Rayleigh–Taylor flow with zero density below, two cases that allow comparison with previous results. Then we use the method for the more general Rayleigh–Taylor instability, with heavy fluid over light, both with positive density. With fixed regularization, the solution appears to converge as the spatial resolution is improved. However, it is not clear that the regularized solution approaches a weak solution.

An interface between two incompressible, inviscid fluids of constant, but possibly different, densities is naturally represented as a vortex sheet, since the jump in tangential velocity results in a concentration of vorticity on the interface. The Birkhoff–Rott formula (2.1) gives the velocity of the interface from this vorticity distribution. This approach remains valid even in the limit of negligible density on one side, as for the case of a liquid–gas interface. Several numerical studies based on these ideas have been made for the Rayleigh–Taylor instability [5,23,39,43]; the motion of water waves [6,12,30,44] (see [44] for a general review); the motion of bubbles or drops [8,31,45]; and vortex sheets with equal densities [25,26]. The literature is extensive, and we will not attempt a comprehensive review here.

In solving the evolution equations numerically for the sheet location and the vortex sheet strength, the main challenge is the evaluation of the Birkhoff–Rott integral by a method that is accurate and numerically stable. For two-dimensional flow the integral can be treated with spectral accuracy by the alternate point trapezoidal rule [3,41], whether the interface is closed (as in a gas bubble) or open and periodic, The success of this approach rests on the ability to remove the singular nature of the integrals completely. However, this accuracy does not overcome the growth of numerical errors arising from the physical instability of two fluid layers with different densities. Moreover, for three-dimensional or axisymmetric flow, high accuracy is very difficult and costly to obtain [7,37,38].

Another approach is to replace the integral by a sum of localized vortices, or vortex blobs, whose size is a numerical parameter to be chosen. In effect, the integral is regularized before being discretized, and the blob size determines the amount of smoothing. This approach has the important advantage that the physical instabilities are controlled, and the numerical parameters can be refined until the regularized solution is completely resolved, as noted by Anderson [1] and Krasny [26]. The main purpose of this paper is to demonstrate that very good accuracy can be achieved with vortex blobs when applied to interfacial motion. We find the results are improved by adjusting the blob size adaptively as the interface deforms. Related methods have been designed [9,11] for the quadrature of singular integrals on surfaces in three dimensions.

Vortex blob methods were introduced as a regularization of the Birkhoff–Rott integral for vortex sheet flows without stratification [16,26,27] in order to provide a numerically stable method for computing the interface motion, despite the Kelvin–Helmholtz instability. (They have also been used for continuous vorticity distributions and in other contexts, especially plasma physics.) Earlier calculations using simple markers or point vortices to represent the vortex sheet resulted in chaotic motion of the markers. Instead of a disordered pattern, vortex blobs form spirals qualitatively like those seen in experiments. Subsequent studies [14,21] have shown that vortex sheet motion is ill-posed, as expected from the linearization of a flat sheet. Moreover, there is now an overwhelming body of evidence, both analytical and numerical, that vortex sheets form curvature singularities in finite time [15,17,20,25,26,35,36,40]. The ill-posedness and singularity formation plague numerical studies and cause round-off errors to contaminate the results [25]. For vortex sheets of one sign, a classical weak solution has been shown to exist beyond the singularity formation time ([18,33]; see also [32]) although its form is unknown, and it is very likely non-unique.

With vortex blob methods, highly refined numerical solutions have been obtained [26], and it has been proved that, in the limit of vanishing blob size, with vorticity of one sign, the numerical solution converges to a weak solution of the actual equations of motion in the form of some spiral [29].

An important value to vortex blob methods, then, is that they permit the calculation of the ill-posed vortex sheet motion with a controlled amount of regularization. This property seems to be important in studies of the Rayleigh–Taylor instability with two fluids of different but positive densities. As the interface deforms, regions of high shear develop on the interface, leading to the formation of a curvature singularity in finite time [4]. A successful adaptation of vortex blob methods to interfacial motion could provide insight into this process by extrapolating from regularized solutions. However, Kerr [23] found that the straightforward use of Krasny blobs [26] was not successful. He introduced additional modifications, such as repositioning of the Lagrangian markers and filtering of the Fourier spectrum, before he could compute beyond the singularity time into the phase where roll-up occurs. Tryggvason [43] used a vortex-in-cell method for the same problem and obtained the roll-up. However, neither of these works clearly established the existence of a regularized solution.

The classical Rayleigh–Taylor instability, a liquid–gas interface with the gas density set to zero, does not appear to exhibit singularity formation [42] except when self-intersection of the the interface occurs. The interface deforms into a pattern of rising gas bubbles and sharp falling liquid spikes with high curvature. With proper care, it is possible to design numerical techniques to calculate the deformation of the interface for long times, until the resolution fails or the interface self-intersects [5,23,45]. This case provides an excellent test for the general method introduced here.

To design accurate blob methods, we replace the singular kernel in the integral by a regularized version, with moment conditions imposed to ensure accuracy [22,28]. In effect the point source of vorticity is replaced by a vortex blob or core of prescribed shape. This view has led to the design of high order accurate vortex methods for smooth fluid flow [13,22]. We follow a similar approach in the design of high order methods for Cauchy integrals on curves, as occur for vortex sheets. In particular, we choose a class of smoothed kernels based on the Gaussian function multiplied by a polynomial. A parameter δ gives the length scale over which the kernel is smoothed, and consequently the length scale of the vortex blob. We then perform a singularity subtraction which is chosen to be exact even with the smoothed integral kernel, so that it does not interfere with the regularization. The resulting integral is then approximated by the trapezoidal rule. The numerical quadrature error depends on the spacing h between Lagrangian markers. When $\delta \ll h$, quadrature errors dominate, and when $\delta \gg h$ smoothing errors dominate.

In Section 2 we state the equations of motion for general interfacial flow, including the specialization to the periodic case. In Section 3 we analyze the smoothing error and find regularized kernels whose smoothing error is $O(\delta^m)$, where $m = 1, 3, 5...$ Estimates of the quadrature error show that it is nominally $O(h)$; a correction to $O(h^3)$ can be computed. Thus, for example, for the kernel with $m = 3$ the corrected error is effectively $O(h^3)$ when we reduce δ and h together with δ/h independent of h. However, the quadrature error can be made negligible by keeping δ larger than the (Eulerian) spacing of the markers. We also derive versions of the regularized kernels for the periodic case.

In Section 4 we test our error analysis and confirm that proper choices lead to high accuracy. We perform a variety of test calculations for the Birkhoff–Rott integral in which the curve is an ellipse and the exact value is known. When the ellipse is almost circular, the errors agree very well with our analysis. However, when the ellipse has a 4-to-1 aspect ratio, the errors downgrade dramatically. The reason is the variation in the local spacing Δs of the points. The errors are dominated by smoothing in regions where δ is much bigger than Δs, whereas quadrature errors are significant where δ is much smaller than Δs. The remedy is simple: we let δ vary along the vortex sheet so that $\delta \approx \Delta s$. We test this idea on the 4-to-1 ellipse and find that the errors are substantially improved. We also verify improvement from using the singularity subtraction and correction when $\delta/\Delta s$ is small. Finally we note that good accuracy results for a wide range of $\delta/\Delta s$ by using the fifth-order kernel with subtraction and correction. Similar results are found for the periodic smoothed kernels.

In Section 5 we apply the new method to several cases of interfacial flow, beginning with the vortex sheet with equal densities, as in Krasny's work [26]. Our first-order regularization, with fixed δ, leads to a spiral roll-up similar to Krasny's but with a tighter spiral for given δ and faster convergence outside. (For further details see [2].) However, the higher order kernels produce a surprisingly different spiral with detailed internal structure. The source of this difference is unclear, but a likely explanation is that the first-order kernels preserve the distinguished sign of the vorticity, whereas the higher order kernels do not. Thus the conclusions about a weak solution may not apply. Next we calculate a Rayleigh–Taylor flow in a liquid–gas interface, using the fifth-order kernel, with δ proportional to Δs, and compare the results with earlier calculations of Baker et al. [5]. The fifth-order convergence is clearly seen. The accuracy is good although it deteriorates over time. This test case provides verification that the present regularized method produces accurate solutions. Finally, we turn to the more difficult case of Rayleigh–Taylor flows with two fluids both of positive density. We use first-order smoothed kernels in the integrals, and we must also use a blob regularization of the vortex sheet strength where it appears in other terms in the evolution equations. Then, for a fixed δ, we can improve the accuracy by increasing spatial and temporal resolution, without any sign of numerical instability. The results indicate the presence of a spiral with an incipient drop of heavier fluid in the middle of the spiral when the density differences are small. For larger density differences, there is the suggestion that multiple drops form along the spiral arm. This level of detail is possible when a Gaussian smoothed kernel is used because the regularization is much more local than in previous efforts. The behavior as $\delta \to 0$ is less clear. We find that outside the spiral region the interface converges as $O(\delta)$, but further detail emerges inside. The vortex sheet strength changes sign on the arms of the spiral, and questions arise about the existence of a weak limit in much the same way as they do for the higher order kernels with the equal-density vortex sheet.

2. Interfacial evolution equations

We consider the motion of an interface between two incompressible, inviscid fluids of constant, but different, densities. We assume the flow is two-dimensional and irrotational, so that the vorticity is confined to a vortex sheet at the interface. We use complex variables and represent the interfacial curve parametrically as $z(\xi,t) = x(\xi,t) + \mathrm{i}y(\xi,t)$. See Fig. 1 for a schematic of the flow.

While the normal component of the velocity must be continuous across the interface for kinematic reasons, the tangential component will jump proportionally to the vortex sheet strength $\gamma(\xi,t)/s_\xi(\xi,t)$ where $s(\xi,t)$ is the arclength along the interface and the subscript ξ refers to its derivative. The average of the velocities of the two fluids at the interface is given by the Birkhoff–Rott integral,

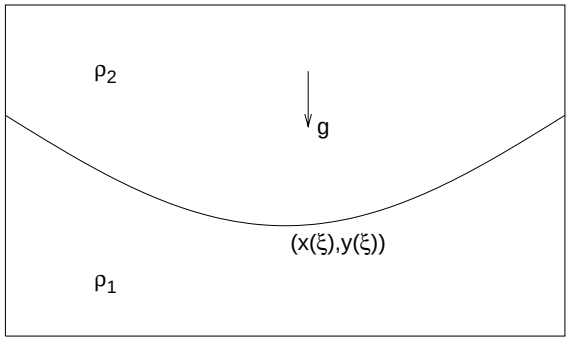

Fig. 1. A schematic of the interface.

$$\overline{q}(\xi,t) \equiv u(\xi,t) - \mathrm{i}v(\xi,t) = \int \gamma(\xi',t)\ K(\xi,\xi')\,\mathrm{d}\xi'. \tag{2.1}$$

In the absence of boundaries or external flow, the kernel is

$$K(\xi,\xi') = \frac{1}{2\pi\mathrm{i}}\ \frac{1}{z(\xi,t) - z(\xi',t)}. \tag{2.2a}$$

The principal value of the integral must be taken, and the over bar denotes complex conjugation.

We are largely concerned with the case of interfacial motion periodic in the horizontal direction. For convenience we assume that the interface is 2π-periodic, with $x(\xi + 2\pi) = 2\pi + x(\xi)$, $y(\xi + 2\pi) = y(\xi)$, and $\gamma(\xi + 2\pi) = \gamma(\xi)$. In this case the range of integration can be reduced to $0 \leqslant \xi' \leqslant 2\pi$ with the periodic kernel, found by the method of images,

$$K(\xi,\xi') = \frac{1}{4\pi\mathrm{i}} \cot\left(\frac{z(\xi,t) - z(\xi',t)}{2}\right). \tag{2.2b}$$

In either case, the motion of the interface is given by

$$\frac{\partial \overline{z}}{\partial t}(\xi,t) = \overline{q}_I(\xi,t) \equiv \overline{q}(\xi,t) + \frac{\alpha}{2}\ \frac{\gamma(\xi,t)}{z_\xi(\xi,t)}. \tag{2.3}$$

A partial derivative with respect to time t is used to emphasize that ξ is kept fixed; the motion is Lagrangian. The subscript ξ denotes the partial derivative with respect to ξ keeping t fixed. The weighting parameter α is introduced to allow an interfacial marker to follow the motion of the upper fluid ($\alpha = -1$), the lower fluid ($\alpha = 1$), or some weighted average of the two. Previous work [4] suggests $\alpha = A$ is a good choice, where A is the Atwood number

$$A = \frac{\rho_1 - \rho_2}{\rho_1 + \rho_2} \tag{2.4}$$

and ρ_1, ρ_2 are the fluid densities below (outside), above (inside) the interface, respectively.

The rate of change of γ is determined by the baroclinic generation of vorticity. The equation below is derived in Baker et al. [6]. (We suppress the arguments ξ, t for readability.)

$$\frac{\partial \gamma}{\partial t} - \frac{\alpha}{2}\left(\frac{\gamma^2}{|z_\xi|^2}\right)_\xi = -2A\left[\mathrm{Re}\left\{z_\xi\ \frac{\partial \overline{q}}{\partial t} - \frac{\alpha}{2}\ \frac{\gamma q_\xi}{z_\xi}\right\} + \frac{1}{8}\ \left(\frac{\gamma^2}{|z_\xi|^2}\right)_\xi + g\ y_\xi\right], \tag{2.5a}$$

where g is the gravitational constant, and

$$\frac{\partial \overline{q}}{\partial t}(\xi) = \int \frac{\partial \gamma}{\partial t}(\xi')K(\xi,\xi')\,\mathrm{d}\xi' + \int \gamma(\xi')\frac{\partial K}{\partial t}(\xi,\xi')\,\mathrm{d}\xi'. \tag{2.5b}$$

For the two choices of the kernel (2.2)

$$\frac{\partial K}{\partial t}(\xi,\xi') = -\frac{1}{2\pi\mathrm{i}}\ \frac{q_I(\xi) - q_I(\xi')}{(z(\xi) - z(\xi'))^2} \tag{2.6a}$$

and

$$\frac{\partial K}{\partial t}(\xi,\xi') = -\frac{1}{8\pi\mathrm{i}}(q_I(\xi) - q_I(\xi'))\ \mathrm{cosec}^2\left(\frac{z(\xi) - z(\xi')}{2}\right). \tag{2.6b}$$

Note that for $A \neq 0$, (2.5) constitutes a Fredholm integral equation of the second kind for $\partial\gamma/\partial t$. When $A = 0$, there is no baroclinic generation of vorticity, and a convenient choice for the weighting parameter is $\alpha = 0$ since γ remains constant in time. Thus for the case of a vortex sheet in one fluid ($A = 0$) the evolution equations are greatly simplified.

The motion of the interface is governed by the following initial-value problem. Given $z(\xi, t)$ and $\gamma(\xi, t)$ at some given time t, we calculate the velocity of the interface through (2.3), (2.1). Next, we solve the Fredholm integral equations for the rate of change of γ (2.5) by Neumann iteration. In Baker et al. [6], it is proved that the Neumann series is globally convergent. Consequently, the location of the interface and γ may be updated through any standard ordinary differential equation solver.

Linearization about equilibrium of two streams shows that the motion is typically ill-posed, i. e., high wavenumber disturbances grow at an unbounded rate (e.g. see [19]). With differing stream velocities at infinity, the Kelvin–Helmholtz instability is present for any A. If the basic flow is at rest, with the heavier fluid above, there are Rayleigh–Taylor instabilities. The prevalence of these instabilities suggests the need for regularization in numerical methods. Nonetheless, direct computations have been successful for classical Rayleigh–Taylor flow with $A = -1$, liquid over gas. The cases $-1 < A < 0$ are different, however, because Kelvin–Helmholtz instabilities form at later time (see [4]).

3. Vortex blob methods

Vortex blob methods are based on replacing the kernel K in (2.1) by a regularized kernel K_δ and then evaluating the integral numerically. Let $e = \overline{q}^{(h)} - \overline{q}$ be the error in this procedure, where $q^{(h)}$ is the numerically calculated velocity. We may decompose the error into two parts $e = e^{(s)} + e^{(h)}$, where

$$e^{(s)}(\xi) = \int \gamma(\xi)\Big(K_\delta(\xi, \xi') - K(\xi, \xi')\Big)\,\mathrm{d}\xi', \tag{3.1a}$$

$$e^{(h)}(\xi) = \int_h \gamma(\xi')\ K_\delta(\xi, \xi')\,\mathrm{d}\xi' - \int \gamma(\xi')\ K_\delta(\xi, \xi')\,\mathrm{d}\xi', \tag{3.1b}$$

where $\int_h$ represents some numerical approximation to the integral. We refer to the two parts $e^{(s)}$ and $e^{(h)}$ as the smoothing and discretization errors, respectively.

We first discuss the choice of the modified kernel and provide an estimate of the smoothing error. The approach is similar to that for the smooth vorticity distributions treated by Beale and Majda [13]. (See also [22]. The case of surface layer potentials was treated by Beale [9,11].) The modified kernel will have the form

$$K_\delta(\xi, \xi') = K(\xi, \xi')\{1 + g(\rho)\}, \quad \rho = |z(\xi) - z(\xi')|/\delta \tag{3.2}$$

with g a real function to be specified and δ a small parameter to be chosen in conjunction with the mesh size h. To ensure that K_δ is smooth, we impose the conditions

$$g(0) = -1, \tag{3.3a}$$

$$g(r) \text{ is a smooth, even function of } r, \quad -\infty < r < \infty \tag{3.3b}$$

Together, (3.3) imply that $g(r) + 1 = \mathrm{O}(r^2)$ as $r \to 0$, so that the denominator in (2.2a) is canceled and K_δ is a smooth function of ξ. In addition, since we wish the modification to be negligible far away, we require

$$g(r) \to 0 \quad \text{rapidly as } |r| \to \infty. \tag{3.3c}$$

To obtain error estimates, we can assume without loss of generality that the point $z(\xi)$ is at the origin of our coordinate system, with $\xi = 0$. For simplicity of notation, we will replace ξ' by ξ. Then the smoothing error becomes

$$e^{(s)} = \int \gamma(\xi)\ K(0,\xi)\ g\left(\frac{|z(\xi)|}{\delta}\right) \mathrm{d}\xi. \tag{3.4}$$

Because of assumption (3.3c), only the contribution for z near 0, say $|z| \leqslant \mathrm{O}(\sqrt{\delta})$, is significant. Thus, we are concerned only with a small part of the interface; we may as well suppose that the coordinates are chosen so that the x-axis lies along the tangent to the interface. This means we may use the parametrization, $x(\xi) = \xi + \hat{x}(\xi)\ \xi^2$, $y(\xi) = \hat{y}(\xi)\ \xi^2$, where $\hat{x}$ and $\hat{y}$ are smooth functions near $\xi = 0$. We replace $g(|z(\xi)|/\delta)$ in (3.4) by $g(|\xi|/\delta)$; we can show by a more careful argument (see [10]), changing the variable of integration to $\mathrm{sgn}(\xi)|z(\xi)|$, that the conclusions below are not affected by this approximation. Thus, (3.4) becomes

$$e^{(s)} = \frac{1}{2\pi} \int g\left(\frac{|\xi|}{\delta}\right)\ \frac{F(\xi)}{\xi}\, \mathrm{d}\xi, \tag{3.5}$$

where F is some smooth function of ξ, provided that γ is smooth. The integration takes place over $|\xi| \leqslant \mathrm{O}(\sqrt{\delta})$; because of (3.3c), the neglected part can easily be shown to be $\mathrm{O}(\delta^p)$ with p large. Again, since g is rapidly decreasing, we may as well extend the integral to infinity.

We will impose further conditions on the function g for the sake of accuracy. Suppose we expand F in a power series about 0;

$$F(\xi) = \sum_{j=0}^{n} a_j \xi^j + R_n(\xi), \quad |R_n(\xi)| \leqslant A_n \xi^{n+1}. \tag{3.6}$$

Then

$$e^{(s)} = \sum_{j=-1}^{n-1} a_{j+1} \int_{-\infty}^{\infty} g\left(\frac{|\xi|}{\delta}\right) \xi^j \,\mathrm{d}\xi + \int_{-\infty}^{\infty} g\left(\frac{|\xi|}{\delta}\right) \frac{R_n(\xi)}{\xi}\, \mathrm{d}\xi. \tag{3.7}$$

Because of the assumption that g is even, the terms with j odd are all zero, including the singular term $j = -1$, taken in the principal value sense. Now let $m - 1 \geqslant 0$ be the order of the first non-vanishing moment of g. Then m is odd, and if $m \geqslant 3$ we have as a further assumption on g

$$\int_{-\infty}^{\infty} g(\xi)\xi^{2k}\,\mathrm{d}\xi = 0, \quad 0 \leqslant 2k \leqslant m-3. \tag{3.8}$$

If (3.8) is violated with $k = 0$, then $m = 1$. We choose $n = m - 1$ in (3.7) so that only the remainder term is left in the expansion. With $p = \xi/\delta$, we have

$$\begin{aligned} |e^{(s)}| &\leqslant A_{m-1} \int_{-\infty}^{\infty} |g(\xi/\delta)|\ \xi^{m-1}\,\mathrm{d}\xi, \\ &= \delta^m\ A_{m-1}\ \int_{-\infty}^{\infty} |g(p)|\ p^{m-1}\,\mathrm{d}p. = C\,\delta^m \end{aligned} \tag{3.9}$$

Since our choice of the origin is arbitrary, we conclude that

$$|e^{(s)}(\xi)| \leqslant C\ \delta^m \tag{3.10}$$

for any point on the interface with C independent of ξ, provided that $z(\xi)$ and $\gamma(\xi)$ have enough bounded derivatives.

We next discuss one class of possible functions g. A simple choice satisfying assumptions (3.3) is $g(r) = -\exp(-r^2)$. Indeed, the corresponding kernel (3.2) is second-order accurate for continuous vorticity distributions. Here, since no moment conditions are satisfied, $m = 1$, and the error (3.10) is first order in δ. To achieve higher order we can search for functions g of the form

$$g(r) = p(r)\exp(-r^2), \tag{3.11}$$

where p is a polynomial in r with only even powers. The proper choices could be found directly by using the moment conditions (3.8) to impose linear constraints on the coefficients of p. However, a simple observation will identify them at once. We recall that the Hermite polynomials can be defined as

$$H_n(r) = (-1)^n \exp(r^2) D^n(\exp(-r^2)), \tag{3.12}$$

where D^n denotes the nth derivative; H_n has degree n and has terms only of the same parity as n. If we set $g(r) = c_n H_n(r)\exp(-r^2)$, with n even, the integral in (3.8) becomes

$$(-1)^n c_n \int_{-\infty}^{\infty} D^n(\exp(-r^2))\; r^{2k}\,\mathrm{d}r, \tag{3.13}$$

after repeated integration by parts this is zero for $2k \leqslant n-2$. To satisfy conditions (3.3) with $m = n+1$, we have only to choose c_n so that $g(0) = -1$, namely, $c_n = -1/H_n(0)$. The first few choices of g in this family are:

$$g_1(r) = -\exp(-r^2), \tag{3.14a}$$

$$g_3(r) = (-1 + 2r^2)\exp(-r^2), \tag{3.14b}$$

$$g_5(r) = \left(-1 + 4r^2 - \frac{4}{3}r^4\right)\exp(-r^2), \tag{3.14c}$$

$$g_7(r) = \left(-1 + 6r^2 - 4r^4 + \frac{8}{15}r^6\right)\exp(-r^2), \tag{3.14d}$$

where the subscript indicates the order of accuracy m in δ, i.e., g_m gives a smoothing error $\mathrm{O}(\delta^m)$.

A similar class of modified kernels, with g a polynomial times a Gaussian, was derived in Beale and Majda [13] for a continuous distribution of vorticity in two dimensions. The polynomials have different coefficients in the two cases, and because of the dimensional difference in the integrals, the order of accuracy is one degree lower in the present case for the same degree of the polynomial. The third-order kernel (3.14b) was used in a test problem for a membrane in inviscid fluid by R. Cortez (unpublished, 1999).

We turn now to the discretization error (3.1b). We begin with an observation concerning quadrature without the δ-modification of the kernel. If the Lagrangian markers are $\{\xi_j\}$ with $\xi_{j+1} - \xi_j = h$, it would be natural to approximate (2.1) by

$$\overline{q}^{(h)}(\xi_l) = h\sum_{j\neq l} \gamma(\xi_j)\; K(\xi_l, \xi_j) \tag{3.15}$$

since the average value of K about its pole is 0. However, this approximation is no better than first order. To see this, we examine the special case where the interface is the x-axis, $z(\xi) = \xi$, $\xi_l = 0$, $h = 1/N$, and γ is 0 outside some interval, say $|\xi| < 1$. Then,

$$\overline{q}(0) = \frac{\mathrm{i}}{2\pi}\int \frac{\gamma(\xi)}{\xi}\,\mathrm{d}\xi \tag{3.16a}$$

and the sum (3.15) is

$$\overline{q}^{(h)}(0) = \frac{\mathrm{i}h}{2\pi} \sum_{j\neq 0} \cdot \frac{\gamma(jh)}{jh} \tag{3.16b}$$

Now let $\zeta(\xi)$ be a smooth, even function such that $\zeta \equiv 1$ for $|\xi| \leqslant 1$ and $\zeta = 0$ for large $|\xi|$. Then $\zeta(\xi)\gamma(\xi) = \gamma(\xi)$ and $\gamma(\xi) - \zeta(\xi)\gamma(0) = \zeta(\xi)[\gamma(\xi) - \gamma(0)]$. To remove the singularity in the integral, we can write

$$\overline{q}(0) = \frac{\mathrm{i}}{2\pi} \int \frac{\zeta(\xi)}{\xi} [\gamma(\xi) - \gamma(0)] \, \mathrm{d}\xi. \tag{3.17a}$$

The added term is zero by symmetry. The integrand in (3.17a) is now a non-singular function whose value at $\xi = 0$ is $\gamma'(0)$. Similarly,

$$\overline{q}^{(h)}(0) = \frac{\mathrm{i}h}{2\pi} \sum_{j\neq 0} \frac{\zeta(jh)}{jh} [\gamma(jh) - \gamma(0)]. \tag{3.17b}$$

It is apparent from (3.17) that $\overline{q}^{(h)}$ is a Riemann sum for $\overline{q}$ with the term $\mathrm{i}h\gamma'(0)/2\pi$ omitted. The Riemann sum itself is high-order accurate, and the quadrature error is therefore $\mathrm{O}(h)$ if $\gamma'(0) \neq 0$. The alternate quadrature of Baker [3] avoids the need for the term at $j = 0$ by using only half the markers, omitting the one at the singularity and alternate ones thereafter. High order accuracy of the desingularized integral is thereby obtained.

If we use the modified kernel K_δ, the integral to be evaluated is

$$\overline{q}_\delta(\xi) = \int \gamma(\xi) K_\delta(\xi, \xi') \, \mathrm{d}\xi. \tag{3.18a}$$

If we discretize with equally spaced points $\xi_j = jh$, the corresponding sum is

$$\overline{q}_\delta^{(h)}(\xi_l) = h \sum_j \gamma(\xi_j) \; K_\delta(\xi_l, \xi_j). \tag{3.18b}$$

(Note that $K_\delta(\xi_l, \xi_l) = 0$.) Then (3.18b) is a Riemann sum for (3.18a), and the quadrature error $e^{(h)}$ has the form

$$e^{(h)} = h \sum_j F(\xi_j) - \int F(\xi) \, \mathrm{d}\xi. \tag{3.19}$$

For $\delta \gg h$, this error is high-order in h, but for $\delta = \mathrm{O}(h)$, the error is no better than $\mathrm{O}(h)$, as will be evident from the analysis that follows. For $\delta \ll h$, the sum (3.18b) reverts to (3.15), and the error is again first order.

In order to deal with this $O(h)$ error in the quadrature of the modified kernel, we will subtract out the principal singularity. This may also improve the accuracy and stability of the computed interfacial motion. However, because of physical instabilities in the motion, it is important that this subtraction be exact. Previously, in Baker et al. [6], the identity

$$\int K(\xi, \xi') z_{\bar{\xi}}(\xi') \, \mathrm{d}\bar{\xi}' = 0 \tag{3.20}$$

is used to remove the singularity in the integrand in the case of a periodic interface. However, with K_δ in place of K, the integral replacing (3.20) is nonzero, although it is $O(\delta)$. Nonetheless, on either a closed curve or periodic curve,

$$\mathrm{Im}\left\{ \int K_\delta(\xi,\xi') z_\xi(\xi')\,\mathrm{d}\xi' \right\} = 0 \tag{3.21}$$

and it is this part that carries the singular integrand. To see that (3.21) holds, we write

$$2\pi K(\xi,\xi') z_\xi(\xi') = A(\xi,\xi') + \mathrm{i}B(\xi,\xi') \tag{3.22}$$

$$A = \left\{ y_\xi(\xi')\Big(x(\xi)-x(\xi')\Big) - x_\xi(\xi')\Big(y(\xi)-y(\xi')\Big) \right\}/r^2, \tag{3.23a}$$

$$B = -\left\{ x_\xi(\xi')\Big(x(\xi)-x(\xi')\Big) + y_\xi(\xi')\Big(y(\xi)-y(\xi')\Big) \right\}/r^2, \tag{3.23b}$$

where

$$r^2 = |z(\xi)-z(\xi')|^2 = \Big(x(\xi)-x(\xi')\Big)^2 + \Big(y(\xi)-y(\xi')\Big)^2. \tag{3.24}$$

Now from (3.2), $K_\delta(\xi,\xi') = K(\xi,\xi') f(r/\delta)$ where $f = 1+g$ and $f(r) = O(r^2)$ as $r \to 0$. Thus,

$$2\pi \mathrm{Im}\Big\{ K_\delta(\xi,\xi') z_\xi(\xi') \Big\} = B(\xi,\xi') f(r/\delta) = \frac{f(r/\delta)}{2r^2} \frac{\mathrm{d}}{\mathrm{d}\xi'}(r^2), \tag{3.25}$$

which is the ξ'-derivative of some function of r^2, and (3.21) follows.

We may use (3.21) to rewrite (3.18a) as

$$\overline{q}_\delta(\xi) = \frac{1}{2\pi\mathrm{i}} \int \left\{ \frac{\gamma(\xi')}{z(\xi)-z(\xi')} + \frac{\gamma(\xi)}{z_\xi(\xi)} B(\xi,\xi') \right\} f\left(\frac{r}{\delta}\right) \mathrm{d}\xi' \tag{3.26}$$

without committing any error. Since $B(\xi,\xi') \sim 1/(\xi'-\xi)$ when ξ' approaches ξ, the expression in braces in (3.26) has no singularity. Our strategy for the numerical calculation of $\overline{q}_\delta$ is to evaluate this integral with standard Riemann sums. We shall identify the largest part of the quadrature error $e^{(h)}$, so that a correction term can be added when it is significant. Corresponding to (3.26), we have the sum

$$\overline{q}^{(h)}_\delta(\xi_l) = \frac{1}{2\pi\mathrm{i}} \sum_j \left\{ \frac{\gamma(\xi_j)}{z(\xi_l)-z(\xi_j)} + \frac{\gamma(\xi_l)}{z_\xi(\xi_l)} B(\xi_l,\xi_j) \right\} f\left(\frac{r_{lj}}{\delta}\right) h, \tag{3.27}$$

where $\xi_j = jh$ and $r_{lj} = |z(\xi_l) - z(\xi_j)|$. We consider the quadrature error $e^{(h)}$ in the limit $\delta, h \to 0$ with δ/h fixed. Beale [11] shows that the largest part of the error is an $O(h)$ term which results from replacing the term in braces in (3.26) by its lowest order approximation at $\xi' = \xi$, and similarly approximating f. After including this correction with the sum (3.27), the remaining error is $O(h^3)$.

We now derive this $O(h)$ correction. For simplicity, we assume again that $\xi = 0$ and $z(0) = 0$, and then replace ξ' by ξ. We also insert a cut-off function $\zeta(\xi)$ with $\zeta \equiv 1$ for ξ near 0 and $\zeta \equiv 0$ for ξ large. Then, for ξ near 0, we can approximate the integrand in (3.26) as

$$\frac{1}{2\pi\mathrm{i}} \left[-\frac{\gamma_\xi(0)}{z_\xi(0)} + \frac{\gamma(0)}{2z_\xi(0)} \left(\frac{z_{\xi\xi}(0)}{z_\xi(0)} + \mathrm{Re}\left\{ \frac{z_{\xi\xi}(0)}{z_\xi(0)} \right\} \right) \right] f\left(\frac{|z_\xi(0)|\xi}{\delta} \right) \zeta(\xi). \tag{3.28}$$

The largest part of the error is therefore

$$e^{(h)} \approx \frac{1}{2\pi \mathrm{i}}\left[-\frac{\gamma_\xi(0)}{z_\xi(0)} + \frac{\gamma(0)}{2z_\xi(0)}\left(\frac{z_{\xi\xi}(0)}{z_\xi(0)} + \mathrm{Re}\left\{\frac{z_{\xi\xi}(0)}{z_\xi(0)}\right\}\right)\right] h\varepsilon^{(h)}, \tag{3.29}$$

where

$$h\varepsilon^{(h)} = h\sum_j f(|z_\xi(0)|jh/\delta)\zeta(jh) - \int f(|z_\xi(0)\xi/\delta)\zeta(\xi)\,\mathrm{d}\xi \tag{3.30}$$

or with $\xi = \eta h$ and $\sigma = \delta/(|z_\xi(0)|h)$,

$$\varepsilon^{(h)} = \sum_j f(j/\sigma)\zeta(jh) - \int f(\eta/\sigma)\zeta(\eta h)\,\mathrm{d}\eta. \tag{3.31}$$

It is proved in [11,10] that we may take the limit as $h \to 0$ and obtain from the Poisson Summation Formula

$$\varepsilon^{(0)} = \lim \varepsilon^{(h)} = \sqrt{2\pi}\ \sigma \sum_{n\neq 0} \hat{g}(2\pi n\sigma), \tag{3.32}$$

where $\hat{g}$ is the Fourier transform

$$\hat{g}(k) = \frac{1}{\sqrt{2\pi}} \int_{-\infty}^{\infty} \mathrm{e}^{-\mathrm{i}k\eta} g(\eta)\,\mathrm{d}\eta. \tag{3.33}$$

As shown in [11], the approximation just obtained accounts for the error up to an $O(h^3)$ remainder, that is,

$$e^{(h)} = \frac{1}{2\pi \mathrm{i}}\left[-\frac{\gamma_\xi(0)}{z_\xi(0)} + \frac{\gamma(0)}{2z_\xi(0)}\left(\frac{z_{\xi\xi}(0)}{z_\xi(0)} + \mathrm{Re}\left\{\frac{z_{\xi\xi}(0)}{z_\xi(0)}\right\}\right)\right] h\varepsilon^{(0)} + O(h^3) \tag{3.34}$$

as $h \to 0$ with δ/h fixed. On the other hand, it can be verified that if $\delta \to 0$ with h fixed, the quadrature reverts to a Riemann sum for the integral with no smoothing; the correction provides the missing term at $j = l$.

The correction (3.29) can be readily computed if $\hat{g}(k)$ is known explicitly and decays rapidly as $k \to \infty$. Such is the case for the family in (3.14):

$$\hat{g}_1(k) = -\frac{\sqrt{2}}{2} e^{-k^2/4}, \tag{3.35a}$$

$$\hat{g}_3(k) = -\sqrt{2}\left(\frac{k}{2}\right)^2 e^{-k^2/4}, \tag{3.35b}$$

$$\hat{g}_5(k) = -\frac{2\sqrt{2}}{3}\left(\frac{k}{2}\right)^4 e^{-k^2/4}. \tag{3.35c}$$

The choice g_3 is especially natural, because the errors from smoothing and discretization are both $O(h^3)$ after the correction when $\delta = O(h)$. With any of the choices in (3.14), it is evident from (3.32) and (3.35) that the correction will be negligible when $\sigma \gg 1$ and $z(\xi)$ and $\gamma(\xi)$ are fairly smooth.

For the case of 2π-periodic vortex sheets, we can obtain smoothed kernels for integration over one period either by summing the kernels just obtained, or by a direct modification of the periodic kernel (2.2b). In the first approach, with the kernel (2.2a) modified by the factor $f = 1 + g$ as above, we sum the periodic images to derive the smoothed kernel on $0 \leqslant \xi' \leqslant 2\pi$

$$\begin{aligned} K_\delta(\xi,\xi') &= \frac{1}{2\pi \mathrm{i}} \sum_{n=-\infty}^{\infty} \frac{1}{z(\xi)-z(\xi')-2n\pi}[1+g(\rho_n)] \\ &= \frac{1}{4\pi \mathrm{i}} \cot\left(\frac{z(\xi)-z(\xi')}{2}\right) + \sum_{n=-\infty}^{\infty} \frac{1}{z(\xi)-z(\xi')-2n\pi} g(\rho_n), \end{aligned} \tag{3.36}$$

where $\rho_n = |z(\xi) - z(\xi') - 2n\pi|/\delta$. Although algebraically tedious, it is straightforward to subtract the sum over images of (3.21) to obtain, with $K_\delta = u - \mathrm{i}v$,

$$\begin{aligned} |z_\xi^2| u = &-\frac{1}{4\pi} \frac{A\sin(\Delta x) + B\sinh(\Delta y)}{\cosh(\Delta y) - \cos(\Delta x)} - \frac{1}{2\pi} \frac{A\Delta x + B\Delta y}{(\Delta y)^2 + (\Delta x)^2} g(\rho_0) \\ &- \frac{1}{2\pi} \sum_{n\neq 0} \frac{A(\Delta x - 2n\pi) + B\Delta y}{(\Delta y)^2 + (\Delta x)^2} g(\rho_n), \end{aligned} \tag{3.37a}$$

$$\begin{aligned} |z_\xi^2| v = &\frac{1}{4\pi} \frac{C\sinh(\Delta y) + D\sin(\Delta x)}{\cosh(\Delta y) - \cos(\Delta x)} + \frac{1}{2\pi} \frac{C\Delta y + D\Delta x}{(\Delta y)^2 + (\Delta x)^2} g(\rho_0) \\ &+ \frac{1}{2\pi} \sum_{n\neq 0} \frac{C\Delta y + D(\Delta x - 2n\pi)}{(\Delta y)^2 + (\Delta x)^2} g(\rho_n), \end{aligned} \tag{3.37b}$$

where $\Delta x = x(\xi) - x(\xi')$, $\Delta y = y(\xi) - y(\xi')$, and

$$\begin{aligned} A &= -\gamma(\xi) y_\xi(\xi) x_\xi(\xi'), \\ B &= \gamma_\xi(\xi') x_\xi^2(\xi) + \Big(\gamma(\xi') y_\xi(\xi) - \gamma(\xi) y_\xi(\xi')\Big) y_\xi(\xi), \\ C &= -\gamma(\xi) x_\xi(\xi) y_\xi(\xi'), \\ D &= \gamma_\xi(\xi') y_\xi^2(\xi) + \Big(\gamma(\xi') x_\xi(\xi) - \gamma(\xi) x_\xi(\xi')\Big) x_\xi(\xi). \end{aligned}$$

Because of the rapid decay of the exponentials, it is not necessary to include terms in the sum beyond $-2 \leqslant n \leqslant 2$. Even so, the above expressions are messy and require many steps to evaluate.

A more direct way to introduce a modified kernel for the periodic case leads to a closed form expression and is therefore easier to use in practice. We set

$$r^2 = 4|\sin(\Delta z/2)|^2 = 2(\cosh(\Delta y) - \cos(\Delta x)) \tag{3.38}$$

and define the periodic smoothed kernel K_δ as in (3.2), with K as in (2.2b), $\rho = r/\delta$, and r given by (3.38) rather than (3.24). We use the same functions g and $f = 1 + g$ as before, except that the meaning of r has changed. Since the new r is periodic, the integrands are periodic. Our theory of the smoothing error applies directly since the singularity at $\xi' = \xi$ is the same and since $r \approx |z(\xi) - z(\xi')|$ for ξ' near ξ. The identity (3.21) still holds because the integrand is again the ξ'-derivative of a smooth function of r^2; this is a consequence of the fact that the periodic kernel K comes from the gradient of the periodic Green's function $(2\pi)^{-1}\log r$. Eqs. (3.22) and (3.23) hold with r^2 given by (3.38), $x(\xi) - x(\xi')$ replaced by $\sin(x(\xi) - x(\xi'))$,

and $y(\xi) - y(\xi')$ replaced by $\sinh(y(\xi) - y(\xi'))$. As a consequence, we can use a subtracted form of this new periodic kernel, analogous to (3.27),

$$\overline{q}_\delta^{(h)}(\xi_l) = \frac{1}{2\pi \mathrm{i}} \sum_j \left\{ \frac{\gamma(\xi_j)}{2} \cot \frac{z(\xi_l) - z(\xi_j)}{2} + \frac{\gamma(\xi_l)}{z_\xi(\xi_l)} B(\xi_l, \xi_j) \right\} f\left(\frac{r_{lj}}{\delta}\right) h \tag{3.39}$$

with r_{lj} defined by (3.38). After the same correction (3.34) as before, the sum (3.39) again has $O(h^3)$ quadrature error.

4. Tests of the numerical quadrature

In this section, we conduct successive tests of our error analysis in the previous section, illustrating the theoretical conclusions and the effects of several alternatives. We find that, with moderate regularization, it is best to choose the smoothing radius δ varying pointwise, taking into account the spacing of the marker points. For most of our tests we integrate over closed curves, so that we calculate smooth versions of the simpler kernel (2.2a). Eventually we check that our conclusions still hold for the periodic case, using smooth versions of (2.2b).

In the series of tests to be described we compute the velocity integral (2.1), (2.2a), choosing the closed curve to be an ellipse. The family of ellipses has the important advantage that the velocity is known exactly for certain γ; in addition, this family allows us to assess the effects of curvature on the errors. The connection between the velocity and the vortex sheet strength along an elliptical curve can be obtained through the use of the conformal mapping $z = \alpha \cosh(\sigma + \mathrm{i}\xi)$. The location of the ellipse is specified by taking σ to be a constant. In particular,

$$z(\xi) = \alpha \cosh\sigma \cos\xi + \mathrm{i}\alpha \sinh\sigma \sin\xi. \tag{4.1}$$

We set the major axis of the ellipse to 1 and determine σ from α by the equation $\alpha \cosh\sigma = 1$, As $\alpha \to 0$, the ellipse becomes a circle, while as $\alpha \to 1$ the ellipse becomes a slit. The curvature is given by

$$\kappa = \frac{\alpha \sinh\sigma}{\left(\sin^2\xi + \alpha^2 \sinh^2\sigma \cos^2\xi\right)^{3/2}}. \tag{4.2}$$

With $\gamma = \sin\xi$, (2.1) becomes

$$\overline{q}(\xi) = \frac{1}{4\alpha}\left(\frac{R + \mathrm{i}I}{D}\right), \tag{4.3}$$

where

$$R = 2e^{-\sigma}(2\sinh^2\sigma\cos^2\xi + e^{-\sigma}\cosh\sigma\sin^2\xi),$$
$$I = \sinh\sigma\sin 2\xi, \quad D = \cosh^2\sigma - \cos^2\xi.$$

For our first tests we use the basic method (3.18b) without singularity subtraction or quadrature correction. Our analysis predicts that the combined error has an $O(h)$ contribution when $\delta \ll h$, but an $O(\delta^m)$ contribution when $\delta \gg h$. In other words, if we keep δ/h fixed, we expect an $O(h)$ error when δ/h is small, and an $O(h^m)$ error when δ/h is large. We first take $\alpha = 0.01$, so that the ellipse is almost a circle. We use the modified kernel (3.2) with $g = g_1$ or g_3 in (3.14). We introduce uniformly spaced points $\xi_j = jh$, $h = 2\pi/N$ and vary δ/h. We measure the error E_h by $\max_j |q(\xi_j) - q_j^{(h)}|$ and show its behavior in Fig. 2 for both g_1 and g_3. By showing $-\log_{10}(E_h)$, we are displaying the number of digits of accuracy. The dashed curves give the

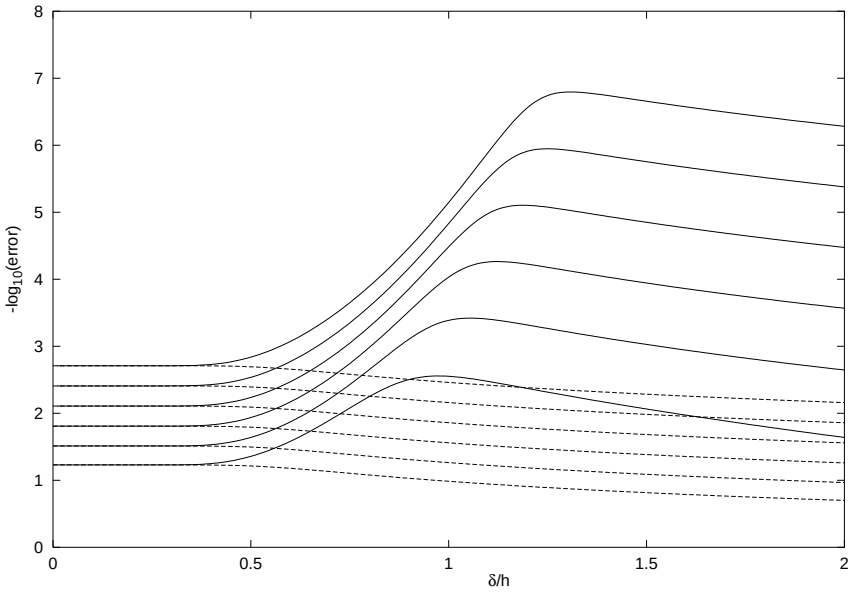

Fig. 2. Errors as δ/h is increased for the smoothed kernels $m = 1$ (dashed) and $m = 3$ (solid). With increasing accuracy, the curves correspond to $N = 16$–512 in powers of 2. The ellipse is almost circular.

results for g_1 as the number of points is doubled, starting at $N = 16$ and ending at 512. The solid curves give the corresponding results for g_3.

For both choices, g_1 and g_3, the effects of δ are not felt for small values of δ/h, and the discretization error $e^{(h)} = O(h)$ dominates as expected. As δ increases beyond h, $e^{(h)}$ decreases exponentially, as seen from (3.32), (3.35) and we see a rapid rise in the number of digits of accuracy. At this stage, the maximum error occurs at $\xi = 0$ (or $\xi = \pi$). As δ approaches the value where the best accuracy is achieved, the location of the maximum error shifts to $\xi = \pi/2$ (or $\xi = -\pi/2$). Now the smoothing error $e^{(s)} = O(\delta^m)$ takes effect, leading to a slow loss of accuracy as δ is further increased. Unfortunately, the optimal choice of δ varies with the level of resolution, but a choice for δ/h around 1.5 still gives very good accuracy.

The apparent even spacing in the curves for small and large values of δ with different resolution N indicates power law behavior in h. If $E_h = C\ h^p$, then

$$E_{\text{diff}} = -\log_{10}(E_{h/2}) + \log_{10}(E_h) = p\log_{10}(2) \approx 0.301\ p. \tag{4.4}$$

In Table 1, we show the errors for $\delta = 0.25h$, and note that $E_{\text{diff}} \sim 0.3$, consistent with the choice $p = 1$. We pick $\delta = 2h$ to examine the behavior for larger δ and the results indicate $p \sim m$, thus confirming the error analysis.

The choice of $\alpha = 0.01$ means that the ellipse is almost circular and the curvature is almost uniform. The spacing between the points is also almost uniform, making the integrands in (3.1) conform almost ideally to the assumptions in the analysis of the errors. As a more practical test, we repeat the first calculation changing to $\alpha = \sqrt{15}/4$, which gives an ellipse with a 4 to 1 aspect ratio. Now the curvature (4.2) varies between 0.25 ($\xi = \pi/2$) and 16.0 ($\xi = 0$). In Fig. 3, we show the maximum error using g_3 as a family of solid curves, each member corresponding to a different resolution: $N = 16$–1024 in powers of 2. The main difference with the results in Fig. 2 is that the transition in behavior from the $O(h)$ error to the $O(h^3)$ error occurs at much smaller values of δ/h; a shift from about 1.3 to 0.3. At the same time, there is a significant

Table 1
Convergence results for two choices of δ

N	$\delta = h/4$		$\delta = 2h$			
	g_1 or g_3		g_1		g_3	
	$-\log_{10}(E_h)$	E_{diff}	$-\log_{10}(E_h)$	E_{diff}	$-\log_{10}(E_h)$	E_{diff}
16	1.229		0.700		1.640	
32	1.511	0.282	0.966	0.266	2.646	1.006
64	1.808	0.296	1.259	0.293	3.567	0.921
128	2.108	0.300	1.558	0.299	4.475	0.907
256	2.408	0.301	1.859	0.301	5.379	0.904
512	2.709	0.301	2.160	0.301	6.282	0.903

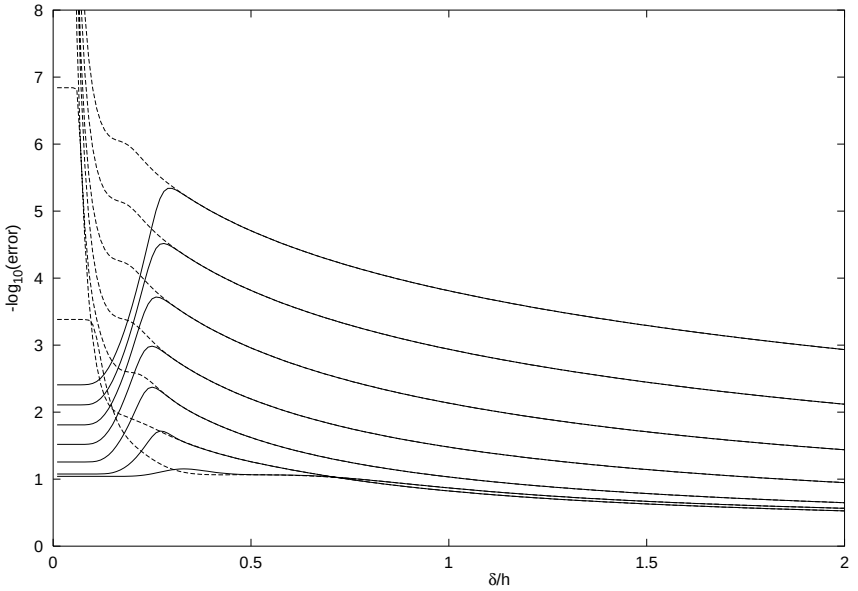

Fig. 3. Errors as δ/h is increased using g_3 for an ellipse with a 4-to-1 aspect ratio. We show results for the basic version (solid curves) and the subtracted and corrected version (dashed curves). The curves increase in resolution from $N = 16$ to $N = 1024$.

drop in accuracy. For $N = 512$, even the best choice of δ/h has an accuracy about two digits worse than the best accuracy for the almost circular test case. This loss of accuracy will be explained further as we proceed.

Now that we have confirmed the general nature of the errors for the basic method (3.18b), we turn to a study of the improvement in the error by using the subtracted sum (3.27) and the $O(h)$ correction term in (3.34). We show the new results as a family of dashed curves in Fig. 3. Clearly shown is the removal of the $O(h)$ for small values of δ/h. Instead, the accuracy improves exponentially. For example, when δ/h is near zero, there are three digits of accuracy for $N = 16$ points, almost 7 digits for $N = 32$, and only round-off errors for the higher resolutions. The dashed curves blend into the solid curves (obtained from the basic method) when the error is dominated by the smoothing of the kernel and the error is $O(h^m)$ for both methods. If we include the subtracted sum and correction term in the earlier case where the ellipse is almost circular, we find that the pattern of curves is very similar to those in Fig. 3 except they are shifted to the right (see Fig. 2, for example).

The reason for the shift in the graphs when the aspect ratio of the ellipse is increased lies in the local spacing where the maximum error occurs. For the deformed ellipse, the maximum error always occurs near $\xi = 0$ (or $\xi = \pi$). Since

$$s_\xi^2 = x_\xi^2 + y_\xi^2 = \sin^2\xi + \alpha^2 \sinh^2\sigma \cos^2\xi, \tag{4.5}$$

the local spacing in arclength at $\xi = 0$ is $\Delta s = s_\xi(0)h = h/4$. If we pick $\delta/h = 0.3$ where the uncorrected results show a maximum, then $\delta/(\Delta s) = 1.2$, a value consistent with the idea that δ should be a little bigger than the local spacing of the points. The implication is that all the curves in Fig. 3 would be stretched to the right by a factor 4 if we used the local spacing $s_\xi h$ instead of h as a scale for δ.

From these observations we are led to consider the smoothed kernel

$$K_\delta(\xi, \xi') = K(\xi, \xi')\{1 + g(\rho)\} \quad \text{with } \rho = \frac{|z(\xi) - z(\xi')|}{\delta_a s_\xi(\xi)}, \tag{4.6}$$

where δ_a is constant. In other words, instead of specifying the blob size δ in terms of the local spacing h in the parametrization variable ($\delta = Ch$), we will make the blob size proportional to the local spacing $\Delta s = s_\xi h$ ($\delta = C_a \Delta s = C_a s_\xi h = \delta_a s_\xi$). In the first case, we pick $C = \delta/h$, and in the second case, we pick $C_a = \delta_a/h$. A re-examination of our error analysis indicates the conclusions are still valid if we replace δ by $\delta_a s_\xi$.

In Fig. 4 we show the results of varying δ_a/h, rather than δ/h for the same test cases as in Fig. 3, with or without the subtraction and correction. As expected, the curves have been shifted to the right. At the same time, there is a dramatic improvement in accuracy.

The advantage of the adaptive δ becomes clear when we consider the possible changes in the shape of the interface during its motion. For example, suppose the vortex sheet were to start as a circle and then move through the family of ellipses as though α were a simple function of time. This motion is not physical, of course, since we are not moving the sheet with the correct velocity, but it does serve to give insight as to the

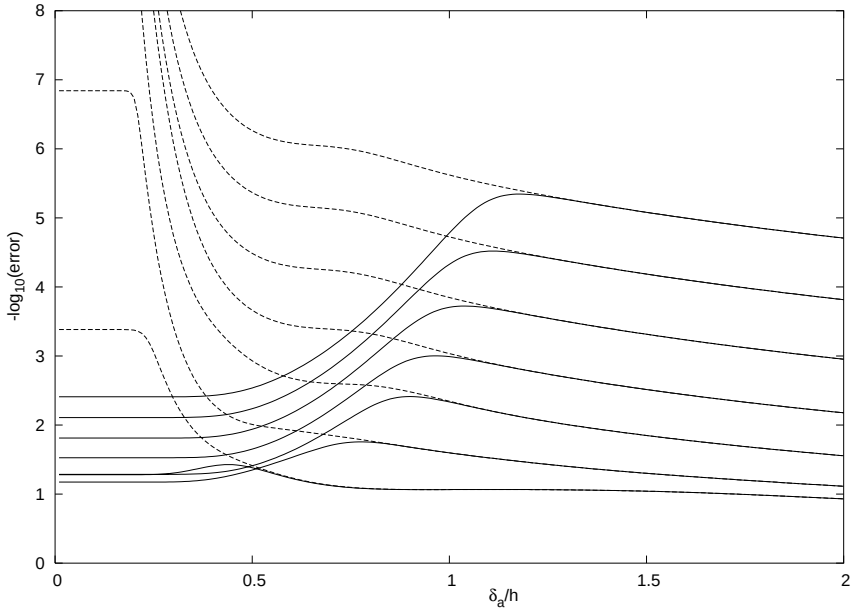

Fig. 4. Errors with adjusted blob size as δ_a/h is increased using g_3 for a 4-to-1 ellipse. We show results for the basic version (solid curves) and the subtracted and corrected version (dashed curves). The curves have resolution from $N = 16$ to $N = 1024$.

potential behavior of the error in the velocity. If we set $\delta = 2h$, then as α increases we see a tremendous loss of accuracy. With $N = 512$, the errors for small times are about 10^{-6} (see Fig. 2). When $\alpha = \sqrt{15}/4$, the errors have increased to about 10^{-2} (see Fig. 4). On the other hand, if we set $\delta_a = 2h$, then the initial error is the same because $s_\xi = 1$, but when $\alpha = \sqrt{15}/4$ the errors will increase to 10^{-4} (see Fig. 4), a far more reasonable increase. We confirm our speculations here in the next section when we consider the motion of an interface during Rayleigh–Taylor instability.

Finally, we consider one more improvement. Even with the subtracted sum (3.27), the correction term from (3.34), and the adjusted δ_a, there is a steady drop-off in the accuracy as δ_a/h increases. This suggests we should replace g_3 by g_5 of (3.14c). There will be no change in the errors for small δ_a/h (they remain exponentially small), but there will be a noticeable improvement for large δ_a/h from $O(h^3)$ to $O(h^5)$. In between where the corrected sum is still important, the errors should remain $O(h^3)$. The results, shown in Fig. 5, support these estimates and, moreover, indicate a reasonable balance in the errors over the range of δ_a/h values. For δ_a/h greater than about 1.2, the errors improve to $O(h^5)$, as evident from the spacing in the curves for the larger values of N. For smaller values of δ_a/h, the errors go through several changes in sign where the spikes in the profiles should go to infinity, but they are truncated due to the frequency by which the data points are plotted. Between $\delta_a/h \approx 0.4$ and ≈ 1.0, the curves appear to be spaced by about 0.9, indicating $O(h^3)$ convergence. For even smaller values of δ_a/h, spectral accuracy dominates.

This concludes our series of tests for closed vortex sheets. Next, we confirm that the same pattern of behavior occurs for periodic sheets in open geometry. Here, we are not aware of a nontrivial test case, so we set the interface at $x(\xi) = \xi + 0.5\sin\xi$, $y(\xi) = 0.5\sin\xi$, and pick the vortex sheet strength as $\gamma(\xi) = 1 - 0.5\cos\xi$. We then calculate the velocity with spectral accuracy by the alternate point quadrature with $N = 512$ points. Comparing with $N = 256$, we conclude the errors are at the level of round-off. Considering these results as "exact", we compute the errors as before; $E_h = \max_j |q(\xi_j) - q_j^{(h)}|$.

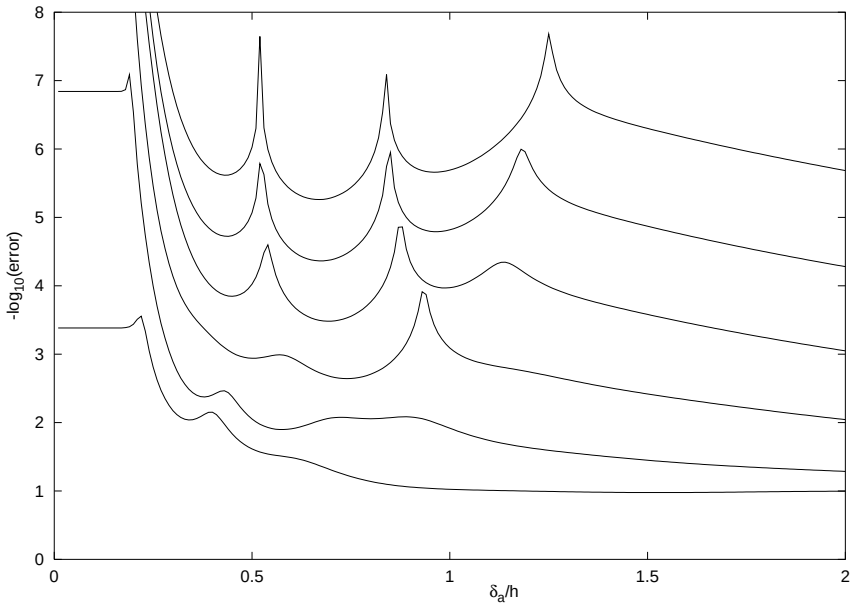

Fig. 5. Errors using g_5 with subtraction/correction as δ_a/h is increased on the 4-to-1 ellipse. The curves increase from $N = 16$ to $N = 512$ in powers in 2.

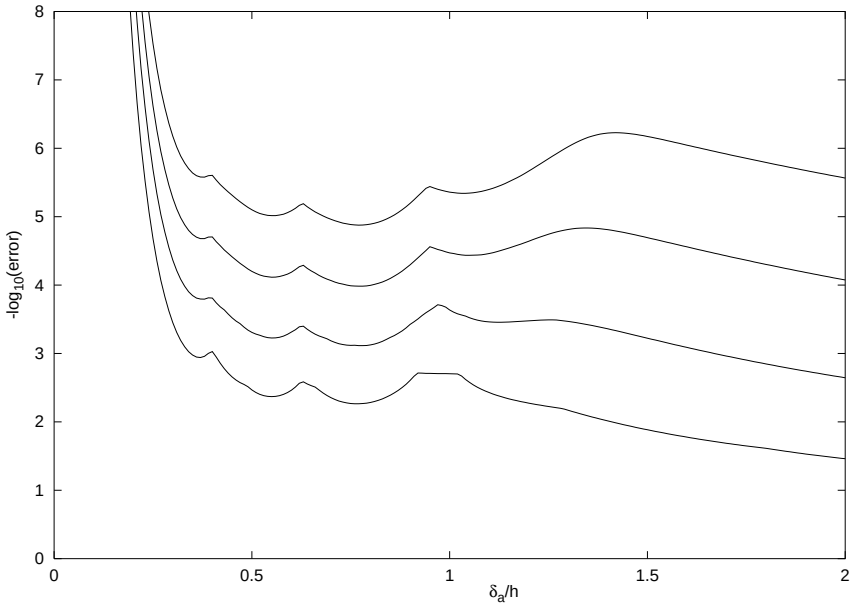

Fig. 6. Errors using the closed form smooth periodic kernel with g_5 and subtraction/correction as δ_a/h is increased. The curves go from $N = 16$ to $N = 128$ in powers of 2.

First, we check that the results of using the periodic form based on summing over images (3.37) shows $O(h)$ behavior when $\delta \ll h$ and $O(h^m)$ convergence (3.10) when $\delta \gg h$. Next, we confirm that the subtracted sum (3.37) with the additional term (3.34) removes the $O(h)$ to give results similar to Fig. 3. Because the interface does not have high curvature or a strong variation in the distribution of points along the curve, we find that the results with a uniform δ have a peak in accuracy slightly below $\delta = h$. The adjusted $\delta = \delta_a s_\xi$ gives better results and shifts the peak in accuracy to just above $\delta_a = h$ as in Fig. 4.

Finally, we test the periodic smoothed kernels defined by multiplying (2.2b) by a function of the periodic r in (3.38). The difference in the results between using the summed kernel (3.37) and the closed form periodic kernel (3.39) is always two or three orders of magnitude less than the error in the results. In other words, there is no difference graphically in plots such as those given in Figs. 2–4 or 5. To illustrate our results, we show the error in Fig. 6 when using the subtracted smooth periodic kernel (3.39) with $g = g_5$ and with the correction (3.34). There is an obvious similarity with Fig. 5.

We conclude from all our tests that using the fifth-order kernel using g_5, with the subtracted and corrected quadrature and with adjusted smoothing radius $\delta = \delta_a s_\xi$, should provide excellent accuracy for a reasonable range of values in δ_a/h. We substantiate our conclusions in the following section by computing several interfacial flows.

5. Application to interfacial motion

We begin with a study of the regularized motion of the classical vortex sheet, with the same fluid density on both sides of the sheet, so that $A = 0$. As usual, we take $\alpha = 0$. Thus there is no vorticity production (cf. (2.5a)) and the velocity in (2.3) reduces to the Birkhoff–Rott integral (2.1). The motion is subject to the Kelvin–Helmholtz instability, with unlimited rate of growth in the high wave numbers. Moreover, there is

strong evidence, both analytic [15,17,34–36] and numerical [25,40] that a vortex sheet will develop curvature singularities in finite time. For these reasons, it is natural to introduce a regularization to compute the motion, as has been done in several studies. Krasny [26] explored thoroughly the effect of one regularization. In the results presented here, we find results similar to Krasny's for a first-order smoothed kernel, but surprisingly different for the higher order kernels.

A typical initial condition for the study of the classical Kelvin–Helmholz instability is

$$x(\xi) = \xi, \quad y(\xi) = 0, \quad \gamma(\xi) = 1 - \varepsilon \cos \xi. \tag{5.1}$$

With $\varepsilon = 0.5$, studies indicate that a curvature singularity forms at $\xi = \pi$ at time $t_s \approx 1.61$. Rigorous theory [18,33] establishes the existence of a weak solution for all time, when the vorticity has a distinguished sign, but the precise nature of the solution is unknown. Moreover, the weak solution may not be unique. One way that this weak solution can be determined is through the limiting behavior of smoothed kernels [29,33]. When the smoothed kernels satisfy certain properties, the limit $\delta \to 0$ will be a weak solution. One of the conditions [29] is that the smoothed kernel is the convolution of the original kernel (2.2a) with a radial blob function. The family (3.14) has this property. However, this condition may not be necessary; in Krasny's work with periodic vortex sheets [26], the regularization is not of this form, but the solutions appear to have a weak limit [26]. Krasny's regularization amounts to replacing r^2, as defined in (3.38), by $r^2 + 2\delta^2$ in the denominator of the periodic velocity kernel. This can be thought of as a particular case of the modification in (3.39) (without subtraction), where $f(r/\delta) = r^2/(r^2 + 2\delta^2) = (r/\delta)^2/((r/\delta)^2 + 2)$. It is reasonable to expect that the regularized periodic kernels of this sort also lead to a weak solution provided the regularized vorticity is of one sign.

In Fig. 7 we compare a vortex sheet with Krasny's regularization (dashed curve) to a similar one using the first-order smoothed Gaussian kernel of (3.14a), with $f = 1 + g_1$ (solid curve). In Krasny's case we take $\delta = 0.057$, while for the Gaussian case $\delta = 0.1$. We start at $t = 0$ using (5.1) with $\varepsilon = 0.5$. We show a blow-up of the vortex sheet near $x = \pi$ at $t = 3.0$. In each case we use N points equally spaced in the parameter ξ

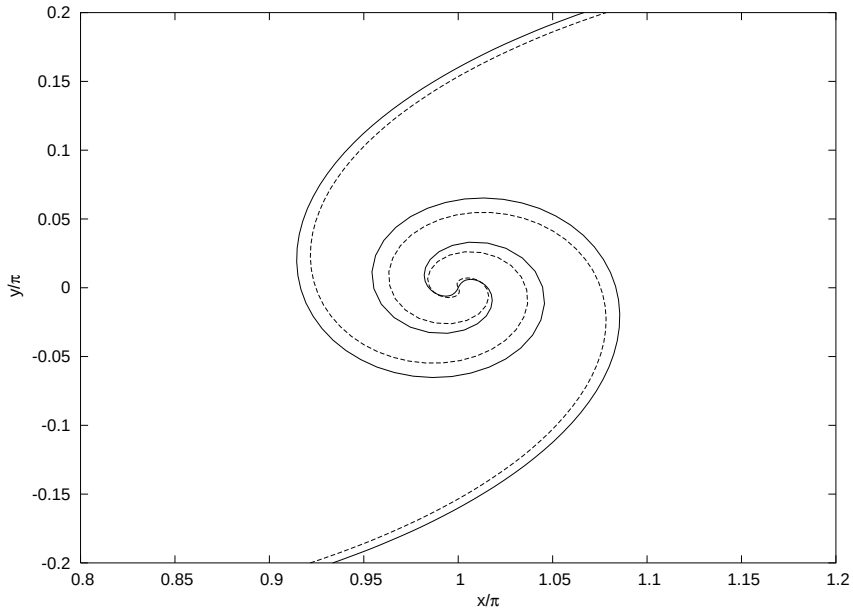

Fig. 7. The roll-up of the vortex sheet using the first-order Gaussian kernel (solid curve) and Krasny's regularization (dashed curve).

with $N = 512$ and a time step of 0.0025 in a standard fourth-order Adams–Moulton predictor–corrector, started with the standard fourth-order Runge–Kutta. Comparison with results of larger time steps and lower resolutions indicate that the results are accurate to better than 10^{-8}.

We obtain the roll-up in Fig. 7 in the Gaussian case using either the periodic kernel from summing over images (3.37) or the closed form periodic kernel (3.39): the maximum difference between the two profiles at $t = 3.0$ and with $\delta = 0.1$ is less than 10^{-4}. We do not bother with the correction terms since, in keeping with common practice, we keep δ fixed and increase N until good accuracy is achieved ($\delta \gg h$). The roll-up is very similar to Krasny's, but comparison is made difficult by the fact that our choice of $\delta = 0.1$ has no direct correspondence to his choices. A detailed comparison will be published elsewhere ([2]).

Next we present calculations of the same vortex sheet problem but regularized with the higher order kernels. In Fig. 8, we show the result of using the third-order kernel with g_3 from (3.14b). The initial condition is again (5.1), and the sheet is shown at the same time $t = 3.0$, with $\delta = 0.1$ and 0.09. For $\delta = 0.1$, we use a time step of 0.0025 and, to keep costs down, we start with $N = 512$ points but double them when the discrete Fourier spectrum is close to saturating (reaching $k = 256$). Repeated doubling occurs at $t = 1.5, 2.25, 2.5$, the final resolution being $N = 4096$. Also, we are forced to use a spectral filter introduced by Krasny [25] to suppress the growth of round-off errors: Fourier amplitudes for x and y below 10^{-12} are set to zero at the completion of each time step. For $\delta = 0.09$, we use the same time step and double the points at $t = 1.5, 2.25, 2.375, 2.75$. Here, the filter level is 10^{-11}.

Similarly, we show in Fig. 9 the results for the fifth-order kernel, with g_5 in (3.14c), at $t = 3.0$ and for $\delta = 0.2, 0.1$. In both cases, we use a time step of 0.0025. For $\delta = 0.2$, we start with $N = 512$ and double points at $t = 2.5$. For $\delta = 0.1$, we double points at $t = 1.5, 2.25, 2.5, 2.75, 2.875$, ending with $N = 16384$ points. The filter level must be set at 10^{-10}.

The first observation is that the spirals are different from those obtained using a first-order kernel. The main spiral is about the same size, but there is much more internal structure, and the appearance of new smaller spirals on the outer arms. The third- and fifth-order kernels have strong similarities: compare $\delta = 0.09$ in the third-order kernel with $\delta = 0.1$ in the fifth-order kernel. There is even some similarity in the internal structures. The amazing detail appears even though the δ's are quite large. If we consider δ as an effective length scale for the smoothing, then the whole spiral falls inside a circle of radius δ. Unfortunately, we are unable to reduce δ much more because of the computation time involved, and we must leave any further study to another time. Nevertheless, the calculations indicate regularized vortex sheet motion with the higher order kernels defined by (3.38), (3.39).

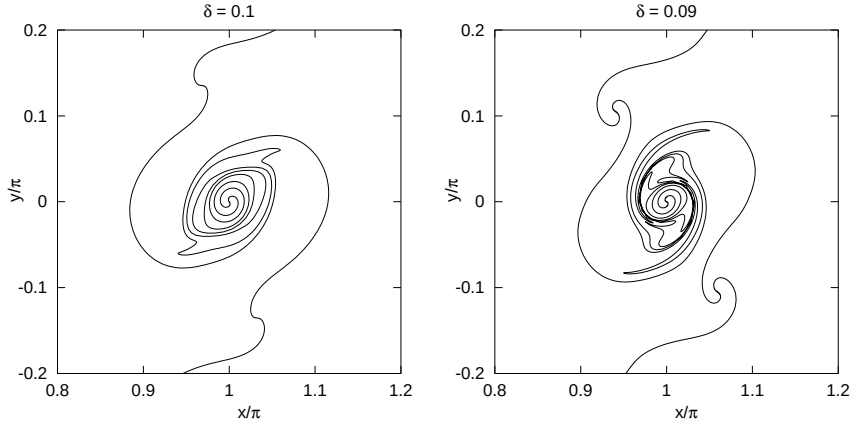

Fig. 8. Location of the vortex sheet – third-order kernel.

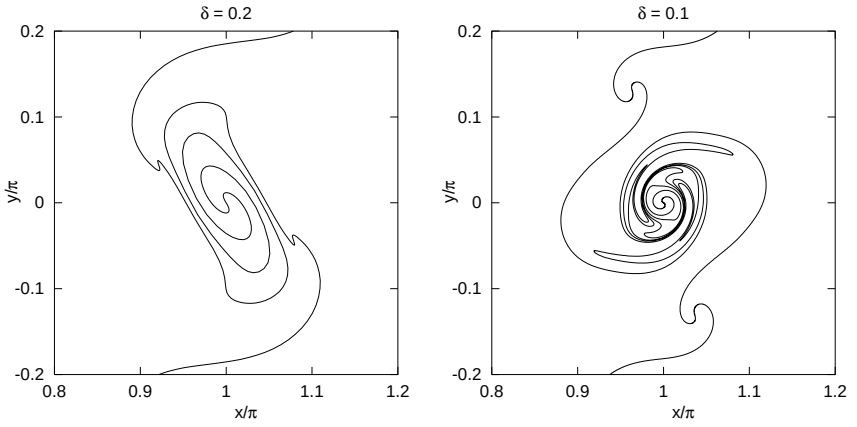

Fig. 9. Location of the vortex sheet – fifth-order kernel.

It is not clear why the regularized vortex sheets with higher order kernels differ so greatly from those with the first-order kernels. A possible explanation is that the first-order kernel with choice g_1 corresponds to a vortex blob which is positive, whereas those of higher order have vorticity of mixed sign. The specified sheet strength (5.1) is positive; it may be that the first-order kernels preserve the special case of sheet strength with distinguished sign, whereas the higher order kernels perturb the problem to the class with mixed sign. The distinguished sign was important in the theory of [18,29,33]. The solutions with higher order kernels might conceivably approximate a different weak solution of the original problem from that of the distinguished sign case, or even a measure-valued solution as suggested in [33]. However, even with the first-order regularization of [26], Krasny and Nitsche [24] have found that chaotic behavior appears inside the spiral at late times after the roll-up.

We now turn to the case of a heavy fluid over a gas with density set to zero, the classical Rayleigh–Taylor instability, corresponding to $A = -1$. The evidence is that the interfacial motion remains regular for all time. The solution can be calculated without the blob regularization, and so this case provides the opportunity to demonstrate the high order accuracy of the kernels (3.14). The evolution is governed by Eqs. (2.1), (2.2b), (2.5), (2.6b), with $A = -1$; we choose $\alpha = -1$, and $g = 1$. To construct numerical solutions with the present blob method, we again use N points evenly spaced in the parameter ξ. The periodic kernels (2.2b), (2.6b) are modified by multiplication with $1 + g(r/\delta)$ where r is given in (3.38). We pick the fifth-order kernel (3.14c) and use the singularity subtraction as in (3.39) and correction given by (3.34), (3.32), (3.35c). We use a Fourier representation to compute derivatives in ξ. We use the Fast Fourier transform to calculate the amplitudes in the Fourier representation, and set to zero all amplitudes below a certain filter level. This helps remove round-off errors in the computation of the derivatives. We also apply this filtering occasionally (every 20th time step) to the profile to help contain the growth of round-off errors. As pointed out in Beale et al. [12], vortex sheet representations of interfacial motion are susceptible to the growth of round-off errors, the more so in the Rayleigh–Taylor because of the natural tendency for modes with smallest length scales to grow the fastest. We use a standard fourth-order Adams–Moulton predictor–corrector to update the interface and the vortex sheet strength. We use a Neumann iteration to solve the integral Eq. (2.5) for $\partial\gamma/\partial t$ and consider it converged when the corrections in the iteration are less than 10^{-7}. For the initial guess, we use a fourth-order polynomial to extrapolate from previous values.

To check the accuracy and reliability of the vortex blob method as just described, we have repeated calculations of the classical Rayleigh–Taylor instability done previously [5]. The initial condition is

$$x(\xi) = \xi, \quad y(\xi) = 0.5\cos\xi, \quad \gamma(\xi) = 0. \tag{5.2}$$

We generate an "exact" solution by using the alternate point quadrature applied to the dipole version of the boundary integral technique as described in Baker et al. [6]. We start with $N = 64$ and calculate up to time $t = 1.6$ with a time step of 0.0025. The filter level is set at 10^{-14} and the integral equation is considered solved when successive iterates fall below 10^{-10} in absolute value. The calculation was stopped when the Fourier amplitudes just below $k = 32$ began to have values above the filter level. The number of points were then doubled through interpolation based on the Fourier series, and the calculation continued to time 2.8 when the Fourier spectrum approached $k = 64$. The filter level had to be raised to 10^{-13}, and then raised again to 10^{-10} to continue the calculations with $N = 256$ points to time 3.8. The final doubling of points allowed us to reach beyond time 4.0. We believe the results for this reference solution have an accuracy of better than 10^{-8}.

We ran the vortex blob codes in two cases, one with the blob size held fixed $\delta = 2h$, and the other with the adjusted blob size $\delta_a = 2h$. We kept N fixed and ran as far as we could with the filter level set at 10^{-10} (as was the convergence criteria for the solution of the integral equation). The time step was set at 0.0025. The largest errors in the calculation occur near the tip of the spike at $x = \pi$. For convenience, we compared the tip of the spike with its "exact" location as an indicator of the error, even though this is a fairly severe measure of the error. We show the results in Fig. 10 as two families of curves, corresponding to different resolution N.

The fifth-order accuracy is clearly observable in the errors in tip location. There is a continual degradation in the accuracy as the spike grows. At early times, the spacing between the marker points is almost uniform, and both families are close in accuracy. As the spike develops, the points cluster toward the tip and the non-uniform spacing causes a significant difference in accuracy between the results for the fixed blob size and the adjusted size. The results confirm that by adjusting δ to the local spacing of the vortex points we gain significant improvement in accuracy for vortex blob methods applied to interfacial motion.

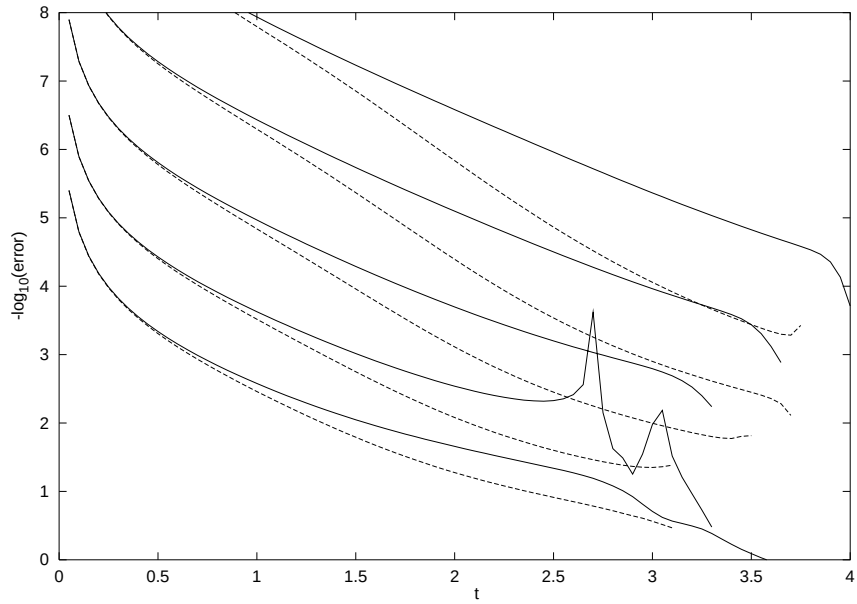

Fig. 10. Errors in Rayleigh–Taylor flow, $A = -1$, as a function of time for different resolutions, $N = 32, 64, 128, 256$. The solid lines are for the case $\delta = 2s_\xi h$; the dashed lines are for the case $\delta = 2h$.

We have confirmed the general pattern in the results for $A > 0$ (internal gravity waves) and, in particular, $A = 1$ (water waves). In our tests, we kept the amplitudes of the waves below that for which wave breaking occurs, but large enough to see the effects of nonlinearity. Since the curvature remains moderate, the improvement from adjusting the vortex blob with the local spacing is less dramatic than in Fig. 10.

Finally we turn to the remaining case of $-1 < A < 0$, with heavy fluid over light, for which the evolution of the interface leads to the formation of a curvature singularity in finite time [4]. This case forces us to consider the influence of the other terms in the equations of motion besides those involving the boundary integrals. Simply smoothing the kernels in the integrals is not enough to avoid the onset of chaotic motion. To obtain regular motion we also need to smooth terms involving the vortex sheet strength. One is the extra term occurring in the velocity (2.3), which determines the tangential velocity of the markers,

$$\frac{\alpha}{2}\frac{\gamma}{z_\xi} = \frac{\alpha}{2}\left(\frac{\gamma}{s_\xi}\right)\frac{\overline{z}_\xi}{s_\xi} \tag{5.3a}$$

and other terms are in the evolution equation (2.5a) for γ,

$$\left(\frac{\alpha}{2} - \frac{A}{4}\right)\frac{\partial}{\partial\xi}\left(\frac{\gamma^2}{s_\xi^2}\right) + A\alpha\left(\frac{\gamma}{s_\xi}\right)q_\xi\frac{\overline{z}_\xi}{s_\xi}. \tag{5.3b}$$

The terms have been written to emphasize the (nonparametric) vortex sheet strength, γ/s_ξ. By smoothing just this quantity in each of the terms above, we find that regularity is restored. If we neglected all the terms in (2.3), (2.5a) but these, we would have a nonlinear hyperbolic system for x_ξ, y_ξ and γ, which typically leads to singularity formation in finite time. Thus it is reasonable to expect singularities to be suppressed by smoothing these terms. (Tryggvason [43] also found that he needed to smooth the vortex sheet strength.)

We smooth the function γ/s_ξ in each occurrence in (5.3) using a blob regularization akin to that in the velocity kernel. We use the smoothing, defined for a generic function f,

$$f_\delta(\xi) = \frac{1}{\delta\sqrt{\pi}}\int_{-\infty}^{\infty} f(\xi')\exp\left(-\frac{|z(\xi) - z(\xi')|^2}{\delta^2}\right)s_\xi(\xi')\,\mathrm{d}\xi'. \tag{5.4}$$

We compute the integral directly with the trapezoidal rule. Because of the rapid decay of the exponential, we need use only a few points on either side of ξ, with $|z(\xi) - z(\xi')|^2 < 30\delta^2$. Since δ will be much larger than h, we do not use a discretization correction. The error in applying the filter will be $O(\delta^2)$. We can easily improve (5.4) to higher order, but here we wish to establish success in regularizing the motion with the simplest choice. Thus we use (5.4) and the first-order smoothing (3.14a) for the velocity integral, with the same value of δ in the two formulas. We again use the periodic velocity kernel in the form (3.39).

The choice of the parameter α affects the resolution of the calculation. An appealing physical choice is to set $\alpha = A$, which picks the tangential velocity to be weighted with the densities. However, the resulting motion crowds points away from the regions where resolution is needed, as observed by Kerr [23]. On the other hand, we find that the choice $\alpha = 0$ works well. There are several reasons why this may be so. First, there is no clear choice for the tangential motion when regularization is used. Second, several of the troublesome terms are removed with $\alpha = 0$; in (5.3), only the first term in (5.3b) remains. Third, the method is more economical since derivatives of q are not needed. Finally, there is a simplification when $f \mapsto f_\delta$ is applied to γ/s_ξ in that s_ξ cancels.

We calculate the motion with two different values of A, starting with $A = -0.2$, which corresponds to fairly weak stratification. This case allows us to demonstrate the effectiveness of the method, since the expected spiral forms. The initial condition is again (5.1) with $\varepsilon = 0.5$. In Fig. 11, we show the location of the interface at $t = 9.0$ for three choices of δ. Making use of symmetry, we show only half the periodic interface for each choice. For $\delta = 0.4$, 0.3, we used $N = 512$ points and a time step of 0.0025. We applied

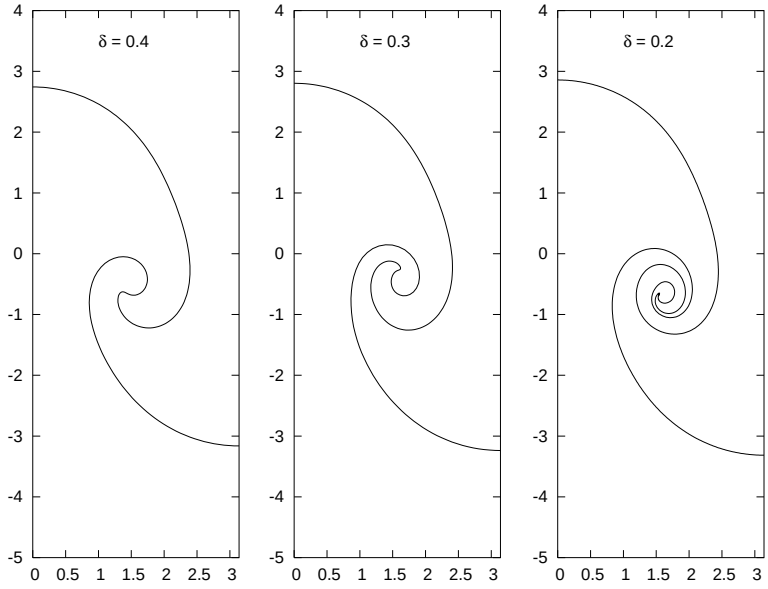

Fig. 11. Location of the interface at time 9.0 with $A = -0.2$ for three choices of δ.

the Krasny Fourier filter with a cut-off level at 10^{-14} to maintain control over round-off errors. For $\delta = 0.2$, we used $N = 512$ up to $t = 6.5$ then doubled the points, and doubled them again at $t = 8.0$. The time step was again 0.0025, but we raised the filter level to 10^{-12}.

There is clear evidence of the formation of a spiral, but it becomes more difficult to resolve with decreasing δ. The reason is the emergence of a drop of heavier fluid at the center, which is likely to be shed in time. Unfortunately, the high curvature of the interface where the drop attaches to the spiral arms requires higher and higher resolution, driving up the cost of the computations. Kerr [23] shows similar behavior for $A = -0.1$.

In Fig. 12 we repeat the calculation with the Atwood ratio changed to $A = -0.5$, so that the stratification becomes strong. Now when the drop forms, it begins to detrain almost immediately, and there is an indication of new drops forming on the arms. To get to the final time $t = 5.75$, we started with $N = 512$ points and successively doubled the number when the tail of the spectrum reached $N/2$. For $\delta = 0.4$, doubling occurred at $t = 5.0$; for $\delta = 0.3$, at $t = 4.5, 5.375$; and for $\delta = 0.2$, at $t = 4.0, 4.625, 5.125$. The Fourier filter level was set at 10^{-14} for the lower resolution runs and increased for the higher resolution runs but never exceeded 10^{-12}. The time step was 0.0025.

With Gaussian smoothed kernels we can see detailed structure in the spiral even with moderate size δ. On the other hand, convergence to a weak solution is less clear. In regions away from the spiral, we can see linear convergence as $\delta \to 0$, in particular, at the lower tip of the falling spike. Inside the spiral, the vorticity has mixed sign, and the emerging detail may be like that for the vortex sheet with $A = 0$ and mixed sign vorticity. As pointed out by Majda [33] for that case, it is possible that there is not a classical weak solution, but rather one in a measure-valued sense. The results also show a scaling in time; that is, if the calculations for $\delta = 0.4$ or 0.3 are continued in time, the location of the sheet appears similar to that for $\delta = 0.2$ at an earlier time, although the size of the spiral is slightly larger.

In conclusion, we have demonstrated that high accuracy can be achieved with vortex blobs in the calculation of two-dimensional interfacial flows where no curvature singularities arise, especially if the blob size is adjusted to the local spacing. Further, we have identified the terms in the equations of motion for

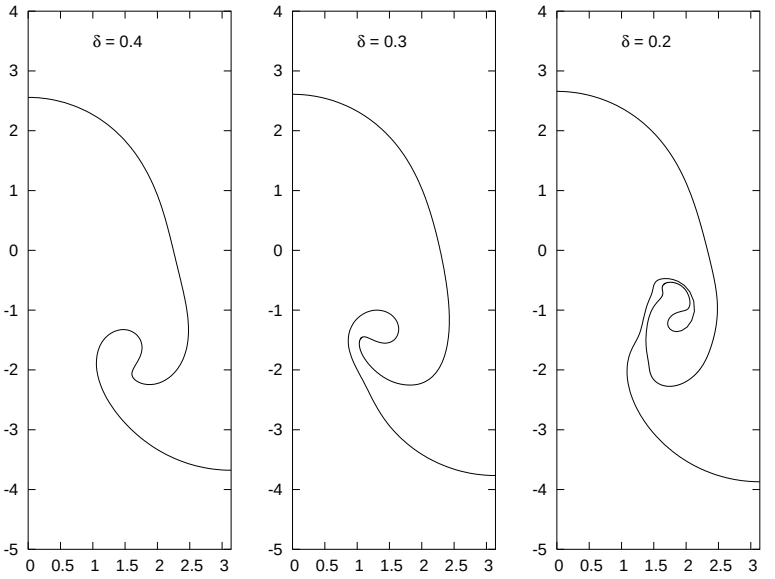

Fig. 12. Location of the interface at time 5.75 with $A = -0.5$ for three choices of δ.

general Atwood ratio that can lead to curvature singularities, and by smoothing them appropriately we can calculate spiral formation. However, questions remain about the convergence as the blob size vanishes. Finally, our approach has a natural extension to three-dimensional motion.

Acknowledgements

Research of the first author was supported by N.S.F. Grant DMS-0112759. Research of the second author was supported by N.S.F. Grant DMS-0102356. We are indebted to Prof. Dan Meiron for several useful discussions.

References

[1] C.R. Anderson, A vortex method for flows with slight density variations, J. Comput. Phys. 61 (1985) 417.
[2] G.R. Baker, L. Pham, in preparation.
[3] G.R. Baker, Generalized vortex methods for free-surface flows, in: R.E. Meyer (Ed.), Waves on Fluid Interfaces, Academic Press, New York, 1983, p. 53.
[4] G.R. Baker, R.E. Caflisch, M. Siegel, Singularity formation during Rayleigh–Taylor instability, J. Fluid Mech. 252 (1993) 51.
[5] G.R. Baker, D.I. Meiron, S.A. Orszag, Vortex simulations of the Rayleigh–Taylor instability, Phys. Fluids 23 (1980) 1485.
[6] G.R. Baker, D.I. Meiron, S.A. Orszag, Generalized vortex methods for free-surface flow problems, J. Fluid Mech. 123 (1982) 477.
[7] G.R. Baker, D.I. Meiron, S.A. Orszag, Boundary integral methods for axisymmetric and three-dimensional Rayleigh–Taylor instability problems, Physica D 12 (1984) 19.
[8] G.R. Baker, D.W. Moore, The rise and distortion of a two-dimensional gas bubble in an inviscid liquid, Phys. Fluids A 1 (1989) 1452.
[9] J.T. Beale, A grid-based boundary integral method for elliptic problems in 3D, SIAM J. Numer. Anal., 2003, accepted for publication.
[10] J.T. Beale, M.-C. Lai, A method for computing nearly singular integrals, SIAM J. Numer. Anal. 38 (2001) 1902.
[11] J.T. Beale, A convergent boundary integral method for three-dimensional water waves, Math. Comput. 70 (2001) 977.

[12] J.T. Beale, T.Y. Hou, J.S. Lowengrub, Convergence of a boundary integral method for water waves, SIAM J. Numer. Anal. 33 (1996) 1797.
[13] J.T. Beale, A.J. Majda, High order accurate vortex methods with explicit velocity kernels, J. Comput. Phys. 58 (1985) 188.
[14] R.E. Caflisch, O.F. Orellana, Long time existence for a slightly perturbed vortex sheet, Commun. Pure Appl. Math. 39 (1986) 1.
[15] R.E. Caflisch, S. Semmes, A nonlinear approximation for vortex sheet evolution and singularity formation, Physica D 41 (1990) 197.
[16] A.J. Chorin, P. Bernard, Discretization of a vortex sheet with an example of roll-up, J. Comput. Phys. 13 (1973) 423.
[17] S.J. Cowley, G.R. Baker, S. Tanveer, On the formation of Moore curvature singularities in vortex sheets, J. Fluid Mech. 378 (1999) 233.
[18] J.-M. Delort, Existence de nappes de tourbillon en dimension deux, J. Am. Math. Soc. 4 (1991) 553.
[19] P.G. Drazin, W.H. Reid, Hydrodynamic Stability, Cambridge University Press, Cambridge, MA, 1981.
[20] J. Duchon, O. Robert, Global vortex-sheet solutions of Euler equations in the plane, J. Diff. Eqns. 73 (1988) 215.
[21] D.G. Ebin, Ill-posedness of the Rayleigh–Taylor and Helmholtz problems for incompressible fluids, Commun. Part. Diff. Eqns. 13 (1988) 1265.
[22] O. Hald, The convergence of vortex methods, II, SIAM J. Numer. Anal. 16 (1979) 726.
[23] R.M. Kerr, Simulation of Rayleigh–Taylor flows using vortex blobs, J. Comput. Phys. 76 (1988) 48.
[24] R. Krasny, M. Nitsche, The onset of chaos in vortex sheet flow, J. Fluid Mech. 454 (2002) 47.
[25] R. Krasny, A study of singularity formation in a vortex sheet by the point vortex method, J. Fluid Mech. 167 (1986) 65.
[26] R. Krasny, Desingularization of periodic vortex-sheet roll-up, J. Comput. Phys. 65 (1986) 292.
[27] K. Kuwahara, J. Takami, Numerical studies of two-dimensional vortex motion by a system of point vortices, J. Phys. Soc. Jpn. 34 (1973) 247.
[28] A. Leonard, Vortex methods for flow simulation, J. Comput. Phys. 37 (1980) 289.
[29] J.-G. Liu, Z. Xin, Convergence of vortex methods for weak solutions to the 2D Euler equations with vortex sheet data, Commun. Pure Appl. Math. 48 (1995) 611.
[30] M.S. Longuet-Higgins, E.D. Cokelet, The deformation of steep surface waves on water, I. A numerical method of computation, Proc. R. Soc. Lond. A 350 (1976) 1.
[31] T.S. Lundgren, N.N. Mansour, Oscillations of drops in zero gravity with weak viscous effects, J. Fluid Mech. 194 (1988) 479.
[32] A.J. Majda, A.L. Bertozzi, Vorticity and Incompressible Flow, Cambridge University Press, Cambridge, MA, 2002.
[33] A.J. Majda, Remarks on weak solutions for vortex sheets with a distinguished sign, Indiana Univ. Math. J. 42 (1993) 921.
[34] D.I. Meiron, G.R. Baker, S.A. Orszag, Analytic Structure of vortex sheet dynamics. I. Kelvin–Helmholtz instability, J. Fluid Mech. 114 (1982) 283.
[35] D.W. Moore, The spontaneous appearance of a singularity in the shape of an evolving vortex sheet, Proc. R. Soc. Lond. A 365 (1979) 105.
[36] D.W. Moore, Numerical and analytical aspects of Helmholtz instability, in: Niordson, Olhoff (Eds.), Theoretical and Applied Mechanics, Proceedings of XVI ICTAM, North-Holland, Amsterdam, 1985, p. 263.
[37] Q. Nie, G.R. Baker, Application of adaptive quadrature to axi-symmetric vortex-sheet motion, J. Comp. Phys. 143 (1998) 49.
[38] M. Nitsche, Axisymmetric vortex sheet motion: accurate evaluation of the principal value integral, SIAM J. Sci. Comput. 21 (1999) 1066.
[39] D.I. Pullin, Numerical studies of surface tension effects in nonlinear Kelvin–Helmholtz and Rayleigh–Taylor instability, J. Fluid Mech. 119 (1982) 507.
[40] M.J. Shelley, A study of singularity formation in vortex-sheet motion by a spectrally accurate vortex method, J. Fluid Mech. 244 (1992) 493.
[41] A. Sidi, M. Israeli, Quadrature methods for periodic singular and weakly singular Fredholm integral equations, J. Sci. Comput. 3 (1988) 201.
[42] S. Tanveer, Singularities in the classical Rayleigh–Taylor flow: formation and subsequent motion, Proc. R. Soc. Lond. A 441 (1993) 501.
[43] G. Tryggvason, Numerical simulation of the Rayleigh–Taylor instability, J. Comput. Phys. 75 (1988) 253.
[44] W. Tsai, D. Yue, Computations of nonlinear free-surface flows, Ann. Rev. Fluid Mech. 28 (1996) 249.
[45] Y. Yang, The initial value problem of a rising bubble in a two-dimensional vertical channel, Phys. Fluids A 4 (1992) 913.